Atmos. Chem. Phys. Discuss., 14, 22793–22836, 2014
www.atmos-chem-phys-discuss.net/14/22793/2014/
doi:10.5194/acpd-14-22793-2014

Atmospheric Chemistry and Physics Discussions

An evaluation of ozone dry deposition in global scale chemistry climate models

C. Hardacre[1], **O. Wild**[1], **and L. Emberson**[2]

[1]Lancaster Environment Centre, Lancaster University, Lancaster, UK
[2]Stockholm Environment Institute, University of York, York, UK

Received: 10 July 2014 – Accepted: 15 August 2014 – Published: 8 September 2014

Correspondence to: C. Hardacre (c.hardacre2@lancaster.ac.uk)

Published by Copernicus Publications on behalf of the European Geosciences Union.

Abstract

Dry deposition to the Earth's surface is an important process from both an atmospheric and biospheric perspective. Dry deposition controls the atmospheric abundance of many compounds as well as their input to vegetative surfaces, thus linking the atmosphere and biosphere. In many atmospheric and Earth system models dry deposition is represented using "resistance in series" schemes developed in the 1980s. These methods have remained relatively unchanged since their development and do not take into account more recent understanding of dry deposition processes that have been gained through field and laboratory based studies. In this study we compare dry deposition of ozone across 15 models which contributed to the HTAP model intercomparison to identify where differences occur. We compare modelled dry deposition of ozone to measurements made at a variety of locations in Europe and North America, noting differences of up to a factor of two but no clear systematic bias over the sites examined. We identify a number of measures that are needed to provide a more critical evaluation of dry deposition fluxes and advance model development.

1 Introduction

Ozone is a significant trace gas constituent in the troposphere. The two main sources of tropospheric ozone are transport from the stratosphere and in situ chemical production via the oxidation of hydrocarbons and CO in the presence of nitrogen oxides (NO_x). Tropospheric O_3, in addition to being a greenhouse gas, is the primary driver of chemical oxidation in the troposphere as a source of OH radicals and is also a potent pollutant in its own right.

Elevated concentrations of O_3 in the troposphere are detrimental to the human respiratory system and to plant health (WHO, 2005; Ashmore, 2005) (and references therein) as it is a strong oxidant. Anenberg et al. (2010) estimated that anthropogenic O_3 pollution was associated with 0.7 ± 0.3 million global deaths annually in the year

ACPD
14, 22793–22836, 2014

2000. Global losses for three major crops have been estimated to be between 11–18 billion USD_{2000} annually for the year 2000 (Avnery et al., 2011a) and are projected to be 12–35 billion USD_{2000} for the year 2030 (Avnery et al., 2011b).

Ozone is primarily removed from the troposphere by chemical destruction and dry deposition to the Earth's surface. Dry deposition processes account for about 25 % of the total O_3 removed from the troposphere (Lelieveld and Dentener, 2000). Because it occurs at the biosphere–atmosphere and ocean–atmosphere interfaces, dry deposition constrains both the near surface O_3 concentration and the input of O_3 to surface ecosystems. In rural areas, dry deposition to terrestrial surfaces drives diurnal variation in surface O_3 (Simpson, 1992). Further, for a reactive and polluting compound such as ozone, understanding the dry deposition process is particularly important for assessing impacts on terrestrial ecosystems.

Dry deposition of O_3 to the terrestrial Earth surface is highly dependent on land cover. Deposition to non-vegetated surfaces is generally slower than deposition to vegetated surfaces (Wesely and Hicks, 2000) and the latter process varies according to plant species and seasonal changes in leaf area index (LAI). At vegetated surfaces, 30–90 % of O_3 dry deposition occurs via the stomata (Fowler et al., 2001; Cieslik, 2004) and is controlled by stomatal conductance, which varies according to species and meteorological conditions. It is uptake of O_3 through the stomata that results in damage to plant tissues, which are subsequently exposed to the highly reactive O_3, negatively impacting plant health.

The strong link between dry deposition, the atmosphere and land cover means that this process is also subject to feedbacks from changes in climate, land use and air pollution (Ainsworth et al., 2012; Fuhrer, 2009). For example, Sanderson et al. (2007) investigated the impact of increasing atmospheric CO_2 on tropospheric O_3 as a result of changes in stomatal conductance. However, despite the importance of dry deposition processes, deposition is one of the most uncertain and poorly constrained aspects of the tropospheric O_3 budget (Wild, 2007). This uncertainty arises from the complexity

ACPD
14, 22793–22836, 2014

and heterogeneity in dry deposition processes which depend on both meteorological conditions near the surface and the characteristics of the surface.

To study O_3 at the global scale it is necessary to use global chemistry transport models (CTMs) or chemistry climate models (CCMs). Uncertainty in dry deposition arises partly from it occurring at sub-grid scales and because the process is heavily parameterized in models (Giannakopoulos et al., 1999; Wesely and Hicks, 2000; Fowler et al., 2009). The global O_3 dry deposition sink is estimated from a wide range of modelling studies to be about 1000 Tg yr^{-1} (Stevenson et al., 2006; Wild, 2007). Of this, approximately one third is deposited to the oceans (Ganzeveld et al., 2009).

Many global scale CTMs parameterize dry deposition using the resistance in series approach developed by Wesely (1989) with additional modifications. This scheme is well characterized and has been previously reviewed, e.g. by Wesely and Hicks (2000); Fowler et al. (2009). The Wesely scheme does not, however, take into account newer understanding of the dry deposition process that has been gained from more recent measurement studies, many of which are summarised in Fowler et al. (2009). Notably the importance of surface wetness, soil moisture, vapour pressure deficit and the role of stomatal versus non-stomatal uptake have been clearly demonstrated. The latter is of particular importance for assessing the impact of O_3 on plants, as it is the uptake of O_3 through the stomata that results in damage to plant tissue (e.g., Reich and Amundson, 1985; Fowler et al., 2001).

Comparatively recent process models such as DO3SE (Emberson et al., 2000b, a, 2001; Buker et al., 2007), which was developed to estimate stomatal ozone flux, do parameterize the effect of soil water deficit and vapour pressure deficit on stomatal conductance. However, these significant developments have not been generally implemented in global scale models.

In this study we assess O_3 dry deposition in global scale CTMs and CCMs to identify the differences between models and to highlight how dry deposition may be evaluated better at the global scale. We used modelled O_3 dry deposition fluxes from a subset of 15 models that contributed to the Task Force on Hemispheric Transport of Air Pollution

ACPD
14, 22793–22836, 2014

(TF HTAP) (Fiore et al., 2009). Results from these models have been used to study nitrogen and sulfur deposition (Sanderson et al., 2008; Dentener et al., 2006) as well as tropospheric ozone (Stevenson et al., 2006) at the global scale, but an assessment of ozone dry deposition has not previously been undertaken.

We describe the methods used to process the model data in Sect. 2. The analysis of modelled O_3 dry deposition is shown in Sects. 3.1 and 3.2. We analyse O_3 deposition fluxes partitioned to land cover classes to evaluate the driving factors for variation in O_3 dry deposition that are associated with land cover across the model ensemble in Sect. 4. Finally, we compare modelled O_3 deposition fluxes to measurements in Sect. 5.

2 Methods

Ozone dry deposition fluxes were diagnosed from a subset of 15 global chemistry transport models that participated in the TF HTAP modelling intercomparison project (further details at http://www.htap.org). These models and the main differences between them are detailed in Sanderson et al. (2008); Dentener et al. (2006); Stevenson et al. (2006). A subset of models from TF HTAP was used as global O_3 dry deposition fluxes were not available from all participating models. Average monthly O_3 dry deposition fluxes from the TF HTAP control runs (Fiore et al., 2009) were used in this study. These control runs (the "SR1 experiment") were driven by meteorological fields from one of several reanalysis centres for the year 2001. The models used in this study are summarized in Table 1.

In most of the models dry deposition of gases was represented using the resistance in series scheme described by Wesely (1989) or a modified version of this scheme. In this type of scheme the dry deposition velocity is determined from Eq. (1):

$$V_d = (R_a + R_b + R_c)^{-1} \quad (1)$$

where the resistance terms R_a, R_b and R_c represent the resistance to transport though the boundary layer, quasi-laminar layer and surface. Although this method is practi-

ACPD
14, 22793–22836, 2014

cal, the properties of the atmosphere and surface can be oversimplified (Wesely and Hicks, 2000). The R_c term may differ considerably between models depending on how the individual surface resistance terms (e.g. stomatal resistance, R_{stom}, and mesophyll resistance, R_m) are represented (Wesely and Hicks, 2000). The initial dry deposition module developed by Wesely (1989) described seven surface resistance terms for 11 land use types and five seasonal categories.

The horizontal resolution of the different models ranged from $1^\circ \times 1^\circ$ to $10^\circ \times 10^\circ$, averaging approximately $3^\circ \times 3^\circ$. Ozone dry deposition from all models was therefore regridded to a common horizontal resolution of $3^\circ \times 3^\circ$ to enable ensemble means and standard deviations to be calculated for each grid box.

To remove first order variation in the simulated O_3 dry deposition fluxes arising from model differences in surface O_3, the fluxes were normalized to allow a more direct comparison of deposition velocities. O_3 dry deposition fluxes were normalized to a surface O_3 of 30 ppb, which is close to the global average surface O_3 concentration (Young et al., 2013). This does not account for second order variation in the dry deposition flux which might arise, for example, from the feedback associated with the decrease in deposition velocity as O_3 is removed from the atmosphere. However, variation as a result of these processes is likely to be small compared with the variation in surface O_3. Throughout this study dry deposition fluxes modified in this way are referred to as "normalised" and the unmodified data are referred to as "modelled". All fluxes are reported here are in $kg\,m^{-2}\,s^{-1}$ where 1×10^{-10} kg O_3 is equivalent to 2.1 nmole O_3.

To better characterise sources of variation in O_3 dry deposition between models the fluxes were partitioned to different land cover classes (LCCs). Modelled monthly O_3 dry deposition was only available as an average flux per grid cell so it was necessary to repartition the fluxes for different land classes. The land cover schemes used in the TF HTAP models differed and described varying degrees of classification, with some schemes including as many as 17 LCCs and others as few as five. The land cover schemes from individual models were not available for this study, so we apply two common schemes to all models. Ozone dry deposition fluxes for individual LCCs were

ACPD
14, 22793–22836, 2014

determined by summing fluxes over grid cells, *i*, scaled by the fractional area, *f*, for that land cover class, *c*, see Eq. (2). Total O_3 deposition per LCC was determined globally over all grid cells and by latitude by summing over separate latitude bands.

$$F_c = \frac{\sum_i F_i \cdot A_i \cdot f_{i,c}}{\sum_i A_i} \quad (2)$$

The modelled O_3 dry deposition fluxes were compared to observed dry deposition fluxes from several sites, primarily located in Europe and America. Seven of these data sets covered periods of more than a year and detailed comparisons between the modelled and observed O_3 dry deposition fluxes were made at these sites. Shorter term measurements were made at a number of other sites. The measurement sites are described in greater detail in Sect. 5.1. The measured O_3 dry deposition fluxes were also compared with modelled fluxes repartitioned for the land cover classes in the grid cell containing the measurement location. The flux to each land cover class at the measurement location was determined assuming the ratio of the fluxes in the grid cell was the same as the ratio of the fluxes at that latitude band.

This approach to repartitioning fluxes for individual LCCs was tested using a single model, the FRSGC/UCI CTM (Wild and Prather, 2000), where land cover specific fluxes were explicitly diagnosed. The repartitioned fluxes were found to be in reasonable agreement with the explicitly diagnosed fluxes, typically within about 10 % over the globe, and within 20 % for all nine land cover classes considered. This gives an indication of the level of uncertainty in the partitioning that can be expected using this approach.

ACPD
14, 22793–22836, 2014

3 Results and discussion

3.1 Global variation in O_3 dry deposition

Annual global O_3 dry deposition fluxes from the 15 TF HTAP models are summarised in Table 1, and the seasonal cycles are shown in Fig. 1 for three distinct latitude bands. The modelled annual global deposition fluxes ranged between 818–1258 Tg yr^{-1} across the models with an ensemble mean ($\pm 1\sigma$) of 978 ± 127 Tg yr^{-1}. The mean, standard deviation and range in the annual global deposition flux across the normalised ensemble were all larger than in the modelled ensemble, with a mean of 1053 ± 187 Tg yr^{-1} and a range of 815–1314 Tg yr^{-1}.

The model mean annual O_3 dry deposition was very similar to that reported in previous modelling studies (Stevenson et al., 2006; Wild, 2007). From global ozone budgets in 15 CTM studies published between 2000 and 2004, Wild (2007) found mean annual global O_3 dry deposition to be 949 ± 222 Tg yr^{-1}. Stevenson et al. (2006) found a mean total annual global O_3 dry deposition of 1003 ± 200 Tg yr^{-1} from 21 models participating in the Atmospheric Composition Change: the European Network of excellence (ACCENT; http://www.accent-network.org) model intercomparison. In the recent Atmospheric Chemistry and Climate Model Intercomparison Project (ACCMIP) mean global O_3 dry deposition was found to be 1094 ± 241 Tg yr^{-1}, based on a sub-set of the participating models (Young et al., 2013).

Monthly O_3 deposition varied by an average of 38 ± 6 Tg month^{-1} across the model ensemble, see Table 1. On average this spread over the models was greater, 46 ± 7 Tg month^{-1}, in the normalised data. The greater range in monthly and annual O_3 dry deposition fluxes indicates that differences in surface O_3 compensate for some of the differences in O_3 dry deposition flux between the models, i.e. that O_3 deposition velocity was more different across the models than the O_3 deposition flux. In contrast, the average seasonal amplitude was greater in the modelled data (38 ± 8 Tg) than in the normalised data (30 ± 10 Tg). This suggests that seasonal variation in surface O_3

ACPD
14, 22793–22836, 2014

accounts for about 20 % of the seasonality in O_3 dry deposition. For individual models, the seasonal amplitude in the normalised fluxes varied from as much as 40 Tg to as little as 12 Tg, highlighting the very different seasonal response in O_3 deposition across the models.

The Wesely scheme describes limited seasonality for surface resistance with smaller resistances to vegetated surfaces in midsummer and spring (Wesely, 1989). The models agree well on the timing of the seasonal cycle (Fig. 1) but differences in seasonality may arise from differences in meteorology or in surface vegetation cover. The effect of the latter is discussed further in Sect. 4.

Figure 1 shows that most O_3 dry deposition occurs in the Tropics and in the Northern Hemisphere (NH) during the growing season. Figure 1a shows that for all the TF HTAP models the most well-defined seasonal cycle in O_3 dry deposition is in the Northern Hemisphere with maximum and minimum deposition during the NH summer and winter respectively. In contrast the seasonal cycles in the Tropics and Southern Hemisphere were much less pronounced. The small difference in the seasonal amplitude between the modelled and normalised data (Fig. 1a and d) further demonstrates that seasonality in the NH is driven by seasonal variation in O_3 dry deposition velocity rather than surface O_3. However, the absence of any seasonal cycle in the Tropics and Southern Hemisphere for the normalised data (Fig. 1e and f) relative to the modelled data (Fig. 1b and c) shows that seasonality in these regions is driven by surface O_3.

3.2 Latitudinal variation in O_3 dry deposition

Total annual O_3 dry deposition per 3° latitude band is shown for the model ensemble in Fig. 2. The peak O_3 dry deposition occurs between 30° S–45° N, see Fig. 2a. In this region the average flux per 3° latitude band is 20–37 Tg yr^{-1} and the range (maximum-minimum) across the ensemble is about 15–20 Tg yr^{-1}, Fig. 2b.

In comparison, the normalized data is more uniform between 30° S–45° N, Fig. 2e and f. The average total deposition per 3° latitude band is about 25 Tg yr^{-1}. The absence of a peak in O_3 dry deposition at 40° N in the normalised data clearly shows that

ACPD
14, 22793–22836, 2014

this is driven by high surface O_3 at these latitudes (Stevenson et al., 2006; Fiore et al., 2009; Young et al., 2013). In contrast, low surface O_3 at tropical latitudes in several models results in high annual dry deposition of up to 50 Tg yr^{-1} O_3 per latitude band in Equatorial regions in the normalised data.

Figure 2 also shows the monthly O_3 dry deposition flux per 3° latitude band for February and August. These highlight both the temporal and spatial variability in global O_3 dry deposition. During February, O_3 dry deposition is greatest between 0°–30° N. The normalised flux shows that this is driven by higher surface O_3 in this region, as the normalised flux is fairly evenly distributed between 30° N–30° S. In August, peak O_3 dry deposition shifts northward to 30° N–45° N. The smaller peak here after normalization shows that high O_3 dry deposition is driven both by increased LAI in the Northern Hemisphere growing season and high summertime surface O_3 at these latitudes (Stevenson et al., 2006; Fiore et al., 2009; Young et al., 2013). A second peak in O_3 deposition, also partly driven by high surface O_3, occurs at 0°–30° S associated with deciduous trees and grassland.

4 O_3 dry deposition to different land cover classes

The greatest variation in O_3 dry deposition occurs between 45° N–30° S, i.e. where vegetated terrestrial land cover is primarily located. To investigate how land cover contributes to variation in O_3 dry deposition across the model ensemble, the fluxes were partitioned to different land cover classes (LCCs) as described in Sect. 2.

Because the native land cover schemes used in the TF HTAP models are not available for this study, data from Olson 1992 (available though: http://acmg.seas.harvard.edu/geos/, Loveland et al., 2000) and the Global Land Cover Facility (GLCF, available from: http://www.landcover.org/, De Fries and Townshend, 1994) are used. This results in some additional uncertainty in the partitioned fluxes, particularly in regions where landcover is very heterogeneous. However, by using two different land cover schemes

ACPD
14, 22793–22836, 2014

for partitioning fluxes across the model ensemble, we gain a clearer picture of the sensitivity of simulated O_3 dry deposition to land cover.

The Olson 1992 data set describes fractional grid cell coverage for 74 LCCs at $1^\circ \times 1^\circ$ resolution. These 74 LCCs were mapped to the 11 Wesely LCCs described in Table 2. The resulting land cover data set is henceforth termed the "OW11" data set. The GLCF data set describes grid cell coverage for 14 LCCs at $1^\circ \times 1^\circ$ resolution, but provides only the dominant LCC in each grid cell. Both data sets were regridded to the same $3^\circ \times 3^\circ$ resolution as the model output. The OW11 and GLCF LCCs and their global coverage are summarized in Table 2.

4.1 Variation in O_3 dry deposition fluxes at homogeneous grid cell locations

Variation in O_3 dry deposition fluxes to individual LCCs was initially compared at 3° grid cells that were dominated by a single land cover class according to the OW11 data set. Normalised monthly O_3 dry deposition fluxes were averaged over all grid cells with 100 % coverage of a single LCC, and these are shown in Fig. 3. Maps showing the locations of these grid cells are shown in the Supplement. In taking this approach, we remove some of the uncertainty associated with using non-native land cover data, as models are likely to be reasonably consistent in their land cover across these regions. This analysis reveals the variability in O_3 dry deposition fluxes to different LCCs across the ensemble. Urban and wetland LCCs were not considered for this analysis as their global coverage is small (Table 2).

Figure 3 shows that seasonality in O_3 dry deposition for the terrestrial vegetated LCCs agrees well across the model ensemble. The only exception is one coarse resolution model which did not include any seasonal variation in O_3 dry deposition. The magnitude of the fluxes generally vary by $1 - -3 \times 10^{-10}$ kg m^2 s^{-1} across the model ensemble, with greatest variation occurring during the NH growing season for all terrestrial vegetated LCCs except tropical forest. O_3 dry deposition to tropical forest was not seasonal and variation across the ensemble was $7 - -8 \times 10^{-10}$ kg m^2 s^{-1} through-

ACPD
14, 22793–22836, 2014

out the year (Fig. 3c). At non-vegetated LCCs (oceans, snow/ice and deserts) there was little ($< 0.5 \times 10^{-10}$ kg m^2 s^{-1}) variation in the O_3 dry deposition fluxes across the ensemble, Fig. 3g–i.

The absence of seasonality in O_3 dry deposition fluxes to tropical forests was likely due to relatively uniform annual LAI compared to other LCCs, such as coniferous forest, deciduous forest, agricultural crop land and tundra, where there are large differences in LAI between the growing and non-growing seasons. Different representation of LAI in the different models is therefore likely to drive much of the observed greater variation in O_3 dry deposition fluxes across the model ensemble during the NH growing season for coniferous forest, deciduous forest, agricultural crop land and tundra. In contrast, variation in O_3 dry deposition fluxes to tropical forest, although large, was relatively consistent throughout the year, Fig. 3c.

For deciduous forest, agricultural crop land and tropical forest particularly high O_3 dry deposition fluxes were observed for two models. For tropical forest, these were driven by low surface O_3, but for deciduous forest and agricultural crop land the O_3 dry deposition velocities appeared to be larger, particularly during the growing season, in these two models.

4.2 Variation in total O_3 dry deposition to land cover classes

Figure 4 shows the total O_3 deposition to LCCs that are described in the OW11 and GLCF land cover data sets. The largest overall sink for O_3 is the oceans, which remove an average of 436 Tg O_3 yr^{-1}, and this is followed by grasslands and deciduous trees which remove 204 and 116 Tg O_3 yr^{-1} respectively, based on fluxes partitioned to the OW11 data set (Fig. 4a). Partitioning to the GCLF data set gives a broadly similar picture, with oceans, wooded grass land and grass land responsible for fluxes of 394 Tg O_3 yr^{-1}, 127 Tg O_3 yr^{-1} and 96 Tg O_3 yr^{-1} respectively.

Deciduous forest is not explicitly classified in the GCLF data set, in contrast to the OW11 data set, and the corresponding area was predominantly considered as wooded

ACPD
14, 22793–22836, 2014

grass land, broad leaf evergreen forest and broad leaf deciduous forest. The greater average O_3 dry deposition to broad leaf evergreen forest (BE) compared with tropical forest, 101 Tg O_3 yr^{-1} and 35 Tg O_3 yr^{-1} respectively, reflects the larger area for BE compared with tropical forest in OW11 (Table 2). Average flux to other LCCs, e.g. crops and coniferous forest were broadly similar for the two land cover data sets.

Figure 4 clearly shows that total global O_3 deposited to oceans is both large and highly variable in the different models. Deposition to oceans is between 263–722 Tg yr^{-1} using the OW11 data set (229–672 Tg yr^{-1} using the GCLF data set), representing a range of about 450 Tg yr^{-1}. Mapping the geographical distribution of O_3 dry deposition fluxes to the oceans showed that differences across the ensemble were spatially uniform. The range in total O_3 deposition to the other LCCs that were large O_3 sinks, e.g deciduous trees and grassland (OW11) and wooded grassland and BE (GCLF), was about 100–130 Tg yr^{-1}.

The lower panels in Fig. 4 show that the variation in the average flux to oceans was small in absolute terms, $< 0.5 \times 10^{-10}$ kg m^{-2} s^{-1}. However, integrating these small differences over the large global area of ocean leads to large differences in total deposition. The sensitivity of surface O_3 to small variations in dry deposition velocity over the oceans was also reported by Ganzeveld et al. (2009), who found that surface O_3 differed by up to 60 % when the O_3 dry deposition velocity was varied between 0.01 and 0.05 cm s^{-1}. Improved characterization of deposition velocities over the ocean would therefore make a substantial contribution to reducing the uncertainty in total global O_3 dry deposition. Further, it is important to constrain the absolute deposition velocities for other LCCs that cover a large area, e.g. for grass land.

Model differences are particularly evident for tropical forest where the range in average O_3 dry deposition flux is 4.5×10^{-10} kg m^{-2} s^{-1}. Tropical forest was not explicitly defined in many of the TF HTAP models used in this study, or in the original Wesely scheme, so it is apparent that a range of O_3 deposition velocities have been applied in these areas across the models. This has less impact for the O_3 dry deposition budget using the OW11 data set, where the tropical forest area is relatively small, but is a large

ACPD
14, 22793–22836, 2014

source of uncertainty when using the GCLF data set. It is important to include a well constrained O_3 dry deposition velocity and global area for tropical forests as observations of between 1.8×10^{-10}–1.9×10^{-9} kg m^{-2} s^{-1} (Rummel et al., 2007) suggest that they are an effective O_3 sink.

This comparison highlights the importance of well constrained O_3 deposition velocities, particularly over water where small differences result in large discrepancies in total O_3 deposition, but also to tropical forests. The importance of land cover classification within models is also emphasized. The differences in fluxes to tropical forests could be greatly reduced by including a specific O_3 deposition velocity for this LCC. The LCC distribution is also shown to be important. For example, the tropical forest and BE LCCs in the OW11 and GCLF data sets cover 0.8 and 2.9 % respectively. A high O_3 dry deposition velocity over these two areas would yield different total deposition and could impact very differently on local atmospheric chemistry and composition.

4.3 Seasonal variation in O_3 dry deposition to land cover classes

The difference in total O_3 dry deposition between the months with highest and lowest deposition, representing the seasonal amplitude, are shown in Fig. 5. The largest seasonal amplitudes are found for deciduous forests, coniferous forests, agricultural crop land, grass land and water in the OW11 data set. Similarly, they are found for coniferous evergreen (CE), mixed coniferous forest (MC), crop land, grass land, high latitude deciduous forest and woodland (HL) and oceans in the GCLF data set.

These differences in the seasonal amplitude of deposition to coniferous, agricultural and high latitude LCCs in both data sets are driven by differences in the seasonal amplitude in O_3 fluxes, shown in the lower panels of Fig. 5. These LCCs also have the largest annual variation in LAI, which is represented differently in the different TF HTAP models, and this contributes to differences in the seasonal amplitude in total O_3 deposition. In contrast, the differences in seasonal amplitude in total O_3 dry deposition for oceans, grass land and deciduous forest are likely due to the large areas covered

ACPD
14, 22793–22836, 2014

by these LCCs as the differences in seasonal amplitude in O_3 dry deposition fluxes for these LCCs is small.

This analysis shows that the amplitude of the seasonal cycle in O_3 dry deposition differs substantially across the models. This is particularly apparent for LCCs that are predominant at northern mid to high latitudes (deciduous forests, coniferous forests, mixed forests, tundra, agricultural and crop land) and grass lands. The seasonal amplitude is expected to be large at northern mid and high latitudes where there is a well defined seasonal cycle in LAI and meteorology. However, the range in seasonal amplitudes suggests that seasonality in vegetation (LAI, etc.) or meteorology is somewhat different within the various TF HTAP models, in agreement with our findings in Sect. 4.1.

Comparison of Figs. 4 and 5 shows that differences in the seasonal amplitude of O_3 dry deposition to individual LCCs across the models remain small compared to the differences in total deposition. However, improved constraints on the seasonal amplitude in fluxes to coniferous forests, mixed coniferous forests, agricultural crop land and high latitude LCCs, in addition to more coherent representation of land cover and LAI across the models would contribute to better agreement between models.

5 Comparison with observed O_3 dry deposition fluxes

5.1 Long term measurement sites

Modelled O_3 deposition fluxes are compared with measured fluxes at seven locations where at least one year of data is available. The measurement sites are summarized in Table 3. Average monthly O_3 dry deposition fluxes were calculated at these sites for comparison with model fluxes. All seven sites are located in the Northern Hemisphere, and hence "summer", "winter" and "growing season" in the following sections refer to NH timings for these periods.

The modelled and observed monthly O_3 dry deposition fluxes are compared in Figs. 6 and 7. At each site the observed monthly fluxes were averaged across a number

ACPD
14, 22793–22836, 2014

of years (measurement period indicated in Table 3) and the simulated monthly fluxes were averaged across the model ensemble. Normalised O_3 dry deposition fluxes and surface O_3 concentrations were also compared at these sites. For each comparison, the seasonality and bias were assessed using the Pearson correlation coefficient and the line of best fit. The seasonality of the observed and modelled O_3 dry deposition fluxes are shown in more detail in Fig. 8 where the average monthly fluxes are shown for each year of measurements and for each model. Measurements from Harvard Forest in 2005 were not available between June and August and were exceptionally low in May, September and November for that year.

At Ulborg, Hyytiala, Harvard Forest, the citrus orchard and Blodgett Forest the correlation coefficients for the comparison between the observed and modelled O_3 dry deposition fluxes are greater than 0.85, indicating that the models are able to capture the seasonal cycle in O_3 dry deposition well at these sites. The lower correlation coefficients at Castel Porziano and Auchencorth Moss reflect a difference in the timing of the peak fluxes in summertime. Observed fluxes were greatest in April and May, whereas the models simulated peak fluxes in June, as shown in Fig. 8.

Normalised O_3 dry deposition fluxes (Fig. 6h) and surface O_3 (Fig. 6i) at Auchencorth Moss suggest that the early peak in O_3 dry deposition is driven by high surface O_3 at this time. At Castel Porziano, surface O_3 in April and May are lower than in summertime indicating that high dry deposition velocities drive the greater springtime fluxes at this site.

The slope of the best fit lines for the modelled and observed O_3 dry deposition fluxes lie between 0.27 and 1.74 across the different measurement sites. Ozone dry deposition fluxes were underestimated at Ulborg, Auchencorth Moss and Blodgett Forest, and overestimated at Harvard Forest and Hyytiala. The best agreement between the modelled and observed fluxes was at the citrus orchard site, where the models slightly overestimated O_3 dry deposition through out the year, although it should be noted that only a single year of data was available for this site. Although the number of sites is

ACPD
14, 22793–22836, 2014

small, we do not find any clear systematic bias in O_3 dry deposition fluxes over the sites as a whole.

We find a greater discrepancy between the modelled and measured O_3 dry deposition fluxes in the growing season than in the winter months at all of the measurement sites except the citrus orchard. These biases do not appear to result from poor simulation of the seasonal cycle in the surface O_3, as this is generally captured well. Rather, it appears that the seasonal amplitude in O_3 dry deposition fluxes is not represented well in the models. For example, at Blodgett Forest the observed fluxes during the growing season are 2–3 times greater than the modelled fluxes over the same period (Fig. 8g). In contrast, at Hyytiala, the modelled growing season fluxes are approximately twice as large as the observed fluxes (Fig. 8d).

Surface O_3 and its seasonal cycle are generally captured well by the model mean at all of the measurement sites. The correlation coefficients lie between 0.73 and 0.94 and the slopes range from 0.46 to 0.97. Consequently, the normalised fluxes do not show a substantial improvement over the modelled fluxes, although these is less seasonal variation in the normalised data as the observed seasonal cycle in surface O_3 is captured well. This suggests that bias between the modelled and observed O_3 dry deposition fluxes is due to the representation of dry deposition velocities rather than bias in surface O_3.

5.2 Partitioned modelled O_3 dry deposition fluxes

Comparing point observations with modelled O_3 dry deposition fluxes presents a number of challenges. Measurement sites may not be representative of the model grid cell, and the grid cell may not provide an accurate representation of the land cover at the site. Figure 9 shows a comparison between observed fluxes and the modelled fluxes partitioned between the various LCCs located in the grid cell in which the measurement site was located. LCC coverage for the model grid cells was obtained from the OW11 land cover data set which described fractional land cover.

ACPD
14, 22793–22836, 2014

It is clear that in some cases the LCC at the measurement site is not represented in the corresponding model grid cell. The Ulborg and Hyytiala measurement sites are situated in coniferous forests, but the OW11 data set does not include coniferous forest in the corresponding grid cells. The partitioned fluxes for deciduous forest and agricultural/crop land at Ulborg, and for deciduous forest, agricultural/crop land and water at Hyytiala are not found to be in better agreement with the observed O_3 dry deposition fluxes than the total modelled flux. Similarly, at Blodgett Forest in California, a deciduous forest site, the land cover classes are desert and grassland, and this partly explains the model understimation of fluxes here.

At Auchencorth Moss, Harvard Forest and the citrus orchard there is better agreement in LCCs between the OW11 data set and the measurement site. At these sites fluxes partitioned to more relevant LCCs are generally in better agreement with the observed fluxes. At Californian orange grove the fluxes to crop land and deciduous forest fit the observed fluxes very well. At Auchencorth Moss, the flux partitioned to crop land is in slightly better agreement with the observations than that due to grassland. At Harvard Forest, the flux partitioned to deciduous forest is higher than that observed, and the flux to coniferous forest is somewhat closer.

We have demonstrated that selecting an appropriate land cover class can lead to improved agreement between modelled and observed O_3 dry deposition fluxes, although this is not always the case. This analysis highlights the difficulties in comparing modelled fluxes with observations, particularly where an appropriate land cover class is unavailable. However, our findings suggest that future comparison of modelled and observed fluxes should be based on model-diagnosed fluxes to the most relevant land cover class within a grid cell using the native LCC scheme in the model, not merely total fluxes at the correct geographical location.

5.3 Short term measurement sites

Modelled O_3 dry deposition fluxes were compared with observations at a number of European sites where short term flux measurements are available, see Table 3. Fig-

ACPD
14, 22793–22836, 2014

ure 10 shows that there is relatively poor agreement between the observed and modelled O_3 dry deposition fluxes at these sites. The average observed O_3 dry deposition flux differed by as much as 6.7×10^{-10} kg m^{-2} s^{-1} between the sites, but this difference is not reflected in the modelled fluxes. However, the regional average observed flux over these sites, $3.8 \times, 10^{-10}$ kg m^{-2} s^{-1}, lies close to the range of the modelled fluxes, $2.8 \pm 1.0 \times 10^{-10}$ kg m^{-2} s^{-1}, suggesting that there is no clear systematic bias in the modelled fluxes over this region.

It is likely that models are unable to capture the spatial variability in O_3 dry deposition at these sites given the $3^\circ \times 3^\circ$ grid resolution used here. The measurement sites represent a range of heterogeneous land cover types, including natural and semi-natural vegetation as well as agricultural and urban areas, within a relatively small geographical region. This heterogeneity is not captured in the OW11 land cover data set, which assigns a similar combination of coniferous tree, deciduous tree, grass land and agricultural/crop land to grid cells in the Western European region. There will be a similar lack of spatial resolution in the native land cover schemes in the models.

The short time scales over which these measurements were made renders it difficult to assess how well the models capture the seasonality at these sites. Measurements at Castel Porziano (Mediterranean pseudosteppe) and Burriana (orange grove) covered two different months in different years. At Burriana the difference in O_3 dry deposition fluxes between May and July was small, in agreement with observations in the Californian citrus orchard. At the Castel Porziano site there was a much greater difference between O_3 dry deposition fluxes observed in May and June in the different years, probably representing meteorological differences over the relatively short observation periods.

The comparison between these observations and the global scale models highlights the difficulty in comparing models with observations, especially in regions with very heterogeneous land cover such as Western Europe. While a finer resolution global or regional-scale model may be able to capture the spatial variability in O_3 dry deposition observed here better, diagnosis of land cover specific fluxes would be valuable to iden-

ACPD
14, 22793–22836, 2014

tify the key weaknesses in current model deposition schemes. Our comparison further highlights the need for spatially representative flux measurements over extended periods (ideally seasonal to annual periods) that are not greatly affected by the short-term variability in meteorology or vegetation properties.

6 Conclusions

This study provides the first analysis of O_3 dry deposition fluxes in global scale chemistry climate models. We identify regions where O_3 dry deposition differs substantially across an ensemble of 15 global models and how land cover drives these differences. We also compare modelled O_3 dry deposition fluxes to observations at a range of measurement sites.

An initial assessment of O_3 dry deposition across latitudes shows that it is most variable between southern and northern mid-latitudes, and the extent of the variation across the models is dependent on the season. The greatest differences in total O_3 dry deposition across the model ensemble occur where deposition velocities and surface O_3 concentrations are highest. The particularly large differences in deposition at tropical latitudes are driven by a small number of models which simulate comparatively low surface O_3 in this region. These results indicate the need for better constraints of O_3 dry deposition during the growing season and at tropical latitudes.

To investigate the causes of the differences in dry deposition across the models, fluxes were partitioned to land cover class. We find that differences in O_3 dry deposition flux to oceans, driven by small absolute differences in dry deposition velocity, are the largest contributor to differences in the global O_3 deposition flux. Over continental regions, deposition to grass lands showed the greatest difference between models. Again, this was driven by relatively small absolute differences in deposition flux integrated over the 8–9 % of the global surface area covered by grassland. Modelled O_3 dry deposition fluxes differed most over tropical forests, suggesting large differences in deposition velocity and the absence of this land cover class in some models.

ACPD
14, 22793–22836, 2014

This comparison of O_3 dry deposition partitioned to LCC demonstrates that differences in total O_3 dry deposition across the models could be greatly reduced by improved constraints on deposition velocities, particularly to oceans, grass lands and tropical forests. The importance of well constrained fluxes to oceans was noted by Ganzeveld et al. (2009) who found that small differences in O_3 dry deposition flux could drive large differences in tropospheric O_3. Differences in O_3 deposition to grass lands or tropical forests will have a much smaller effect on the global tropospheric O_3 burden, but may significantly impact local atmospheric composition.

We highlight the importance of agreement in the land cover classification used in global scale models. Some models use very limited land cover schemes with as few as five LCCs, and this may be a particular problem for simpler Earth System Models where vegetation processes are explicitly simulated online. This results in some LCCs, e.g. tropical forest, being omitted altogether. Further, deposition flux measurements are available from a relatively limited range of land cover classes, so differences in mapping these to the native LCC scheme leads to differing global coverage and deposition in different models. This may lead to substantial differences in local surface O_3 even though the global O_3 burden is not greatly affected. Tropical forests are important regions for atmospheric processing, for example, and observations have shown that O_3 dry deposition is relatively fast in these locations. Application of a generic "deciduous forest" to this land cover therefore results in underestimation of O_3 deposition fluxes and a systematic bias in the chemical environment here.

We do not have sufficient data from the HTAP model study to assess the impact of other biases which are likely to drive model differences in O_3 dry deposition. Biases in the diurnal cycle of deposition fluxes and partitioning between stomatal and non-stomatal fluxes are likely to be cumulative across large areas and may have a significant effect on global annual O_3 dry deposition. While O_3 dry deposition has not previously been reported at this level of detail, we recommend that future model comparisons request these additional flux diagnostics to allow deposition processes to be tested more thoroughly.

ACPD
14, 22793–22836, 2014

In this study we make the first assessment of O_3 dry deposition fluxes in global models against observations. The models generally simulate the seasonal variations in O_3 dry deposition fluxes well. While it is difficult to assess the overall performance of the models based on the relatively limited observations available, we do not see a systematic bias in the models over these locations. In general, we find that the discrepancy between modelled and observed O_3 dry deposition fluxes is driven by the modelled O_3 dry deposition velocity rather than by surface O_3, but this was not the case at all sites.

This comparison between the models and observations provides an initial set of metrics that can be used as a simple indicator of model performance. More critical testing of model performance will require more detailed diagnostics of O_3 dry deposition, including fluxes partitioned by land cover class, stomatal and non-stomatal fluxes, and fluxes at higher temporal resolution to explore the diurnal behaviour. It will also be important to have long-term flux measurements, over at least a full seasonal cycle, from sites with land cover classes that are broadly representative of a wider region. Characterization of deposition velocities over a wide range of land cover classes would be particularly valuable for refining the variables used in current model resistance schemes, including over the ocean where differences between models are large. These should allow us to place better constraints on this important term in the global O_3 budget.

The Supplement related to this article is available online at doi:10.5194/acpd-14-22793-2014-supplement.

Acknowledgements. This work was supported by the Natural Environment Research Council as part of the Atmospheric Chemistry in the Earth System (ACITES) network. We acknowledge the modelling groups who contributed to the HTAP model intercomparison project and provided the model results we have used in this study. We are also grateful to the following for generously allowing their valuable measurement data to be used here: Nuria Altimir (University of Helsinki, Finland), Stanislaw Cieslik (formerly at the Joint Research Centre), Mhairi Coyle (Centre for Ecology and Hydrology, Edinburgh), Silvano Fares (Agricultural Research Council, Italy), Allen

ACPD
14, 22793–22836, 2014

Goldstein (University of California at Berkeley, CA, USA), Teis Mikkelsen (Technical University of Denmark, Denmark) and Bill Munger (Harvard University, MS, USA).

References

Ainsworth, E. A., Yendrek, C. R., Sitch, S., Collins, W. J., and Emberson, L. D.: The effects of tropospheric ozone on net primary productivity and implications for climate change, Annu. Rev. Plant Biol., 63, 637–661, doi:10.1146/annurev-arplant-042110-103829, 2012. 22795

Anenberg, S. C., Horowitz, L. W., Tong, D. Q., and West, J. J.: An estimate of the global burden of anthropogenic ozone and fine particulate matter on premature human mortality using atmospheric modeling, Environ. Health Persp., 118, 1189–1195, doi:10.1289/ehp.0901220, 2010. 22794

Ashmore, M. R.: Assessing the future global impacts of ozone on vegetation, Plant Cell Environ., 28, 949–964, doi:10.1111/j.1365-3040.2005.01341.x, 2005. 22794

Avnery, S., Mauzerall, D. L., Liu, J., and Horowitz, L. W.: Global crop yield reductions due to surface ozone exposure: 1. Year 2000 crop production losses and economic damage, Atmos. Environ., 45, 2284–2296, doi:10.1016/j.atmosenv.2010.11.045, 2011a. 22795

Avnery, S., Mauzerall, D. L., Liu, J., and Horowitz, L. W.: Global crop yield reductions due to surface ozone exposure: 2. Year 2030 potential crop production losses and economic damage under two scenarios of {O3} pollution, Atmos. Environ., 45, 2297–2309, doi:10.1016/j.atmosenv.2011.01.002, 2011b. 22795

Bey, I., Jacob, D. J., Yantosca, R. M., Logan, J. A., Field, B. D., Fiore, A. M., Li, Q. B., Liu, H. G. Y., Mickley, L. J., and Schultz, M. G.: Global modeling of tropospheric chemistry with assimilated meteorology: model description and evaluation, J. Geophys. Res.-Atmos., 106, 23073–23095, doi:10.1029/2001JD000807, 2001. 22823

Buker, P., Emberson, L. D., Ashmore, M. R., Cambridge, H. M., Jacobs, C. M. J., Massman, W. J., Muller, J., Nikolov, N., Novak, K., Oksanen, E., Schaub, M., and de la Torre, D.: Comparison of different stomatal conductance algorithms for ozone flux modelling, Environ. Pollut., 146, 726–735, doi:10.1016/j.envpol.2006.04.007, 2007. 22796

Cieslik, S.: Ozone uptake by various surface types: a comparison between dose and exposure, Atmos. Environ., 38, 2409–2420, doi:10.1016/j.atmosenv.2003.10.063, 2004. 22795, 22825

ACPD
14, 22793–22836, 2014

Cieslik, S. and Labatut, A.: Ozone surface fluxes and stomatal activity, in: Proceedings of Eurotrac Symposium '96 – Transport and Transformation of Pollutants In the Troposphere, Vol. 2: Emissions, Deposition, Laboratory Work and Instrumentation, BMW AG; European Commiss; Ford Res Labs; Marktgemeinde, GarmischEOLEOLPartenkirchen; Mercedes Benz, 25–29 March 1996, Garmisch-Patenkirchen, 177–184, 1997. 22825

Collins, W., Stevenson, D., Johnson, C., and Derwent, R.: Tropospheric ozone in a global-scale three-dimensional lagrangian model and its response to NO_X Emission Controls, J. Atmos. Chem., 26, 223–274, doi:10.1023/A:1005836531979, 1997. 22823

Collins, W. J., Bellouin, N., Doutriaux-Boucher, M., Gedney, N., Halloran, P., Hinton, T., Hughes, J., Jones, C. D., Joshi, M., Liddicoat, S., Martin, G., O'Connor, F., Rae, J., Senior, C., Sitch, S., Totterdell, I., Wiltshire, A., and Woodward, S.: Development and evaluation of an Earth-System model – HadGEM2, Geosci. Model Dev., 4, 1051–1075, doi:10.5194/gmd-4-1051-2011, 2011. 22823

De Fries, R. S. and Townshend, J. R. G.: Ndvi-derived Land-cover classifications at a global-scale, Int. J. Remote Sens., 15, 3567–3586, 1994. 22802

Dentener, F., Drevet, J., Lamarque, J. F., Bey, I., Eickhout, B., Fiore, A. M., Hauglustaine, D., Horowitz, L. W., Krol, M., Kulshrestha, U. C., Lawrence, M., Galy-Lacaux, C., Rast, S., Shindell, D., Stevenson, D., Van Noije, T., Atherton, C., Bell, N., Bergman, D., Butler, T., Cofala, J., Collins, B., Doherty, R., Ellingsen, K., Galloway, J., Gauss, M., Montanaro, V., Mueller, J. F., Pitari, G., Rodriguez, J., Sanderson, M., Solmon, F., Strahan, S., Schultz, M., Sudo, K., Szopa, S., and Wild, O.: Nitrogen and sulfur deposition on regional and global scales: a multimodel evaluation, Global Biogeochem. Cy., 20, GB4003, doi:10.1029/2005GB002672, 2006. 22797

Emberson, L. D., Ashmore, M. R., Cambridge, H. M., Simpson, D., and Tuovinen, J. P.: Modelling stomatal ozone flux across Europe, Environ. Pollut., 109, 403–413, doi:10.1016/S0269-7491(00)00043-9, 2000a. 22796

Emberson, L. D., Wieser, G., and Ashmore, M. R.: Modelling of stomatal conductance and ozone flux of Norway spruce: comparison with field data, Environ. Pollut., 109, 393–402, doi:10.1016/S0269-7491(00)00042-7, 2000b. 22796

Emberson, L. D., Ashmore, M. R., Simpson, D., Tuovinen, J. P., and Cambridge, H. M.: Modelling and mapping ozone deposition in Europe, Water Air Soil Pollut., 130, 577–582, doi:10.1023/A:1013851116524, 2001. 22796

ACPD
14, 22793–22836, 2014

Fares, S., Park, J.-H., Ormeno, E., Gentner, D. R., McKay, M., Loreto, F., Karlik, J., and Goldstein, A. H.: Ozone uptake by citrus trees exposed to a range of ozone concentrations, Atmos. Environ., 44, 3404–3412, doi:10.1016/j.atmosenv.2010.06.010, 2010. 22825

Fares, S., Weber, R., Park, J.-H., Gentner, D., Karlik, J., and Goldstein, A. H.: Ozone deposition to an orange orchard: partitioning between stomatal and non-stomatal sinks, Environ. Pollut., 169, 258–266, doi:10.1016/j.envpol.2012.01.030, 2012. 22825

Fares, S., Savi, F., Muller, J., Matteucci, G., and Paoletti, E.: Simultaneous measurements of above and below canopy ozone fluxes help partitioning ozone deposition between its various sinks in a Mediterranean Oak Forest, Agr. Forest Meteorol., submitted, 2014. 22825

Fiore, A. M., Dentener, F. J., Wild, O., Cuvelier, C., Schultz, M. G., Hess, P., Textor, C., Schulz, M., Doherty, R. M., Horowitz, L. W., MacKenzie, I. A., Sanderson, M. G., Shindell, D. T., Stevenson, D. S., Szopa, S., Van Dingenen, R., Zeng, G., Atherton, C., Bergmann, D., Bey, I., Carmichael, G., Collins, W. J., Duncan, B. N., Faluvegi, G., Folberth, G., Gauss, M., Gong, S., Hauglustaine, D., Holloway, T., Isaksen, I. S. A., Jacob, D. J., Jonson, J. E., Kaminski, J. W., Keating, T. J., Lupu, A., Marmer, E., Montanaro, V., Park, R. J., Pitari, G., Pringle, K. J., Pyle, J. A., Schroeder, S., Vivanco, M. G., Wind, P., Wojcik, G., Wu, S., and Zuber, A.: Multimodel estimates of intercontinental source-receptor relationships for ozone pollution, J. Geophys. Res.-Atmos., 114, D04301, doi:10.1029/2008JD010816, 2009. 22797, 22802

Fowler, D., Flechard, C., Cape, J. N., Storeton-West, R. L., and Coyle, M.: Measurements of ozone deposition to vegetation quantifying the flux, the stomatal and non-stomatal components, Water Air Soil Pollut., 130, 63–74, doi:10.1023/A:1012243317471, 2001. 22795, 22796, 22825

Fowler, D., Pilegaard, K., Sutton, M. A., Ambus, P., Raivonen, M., Duyzer, J., Simpson, D., Fagerli, H., Fuzzi, S., Schjoerring, J. K., Granier, C., Neftel, A., Isaksen, I. S. A., Laj, P., Maione, M., Monks, P. S., Burkhardt, J., Daemmgen, U., Neirynck, J., Personne, E., Wichink-Kruit, R., Butterbach-Bahl, K., Flechard, C., Tuovinen, J. P., Coyle, M., Gerosa, G., Loubet, B., Altimir, N., Gruenhage, L., Ammann, C., Cieslik, S., Paoletti, E., Mikkelsen, T. N., Ro-Poulsen, H., Cellier, P., Cape, J. N., Horvath, L., Loreto, F., Niinemets, U., Palmer, P. I., Rinne, J., Misztal, P., Nemitz, E., Nilsson, D., Pryor, S., Gallagher, M. W., Vesala, T., Skiba, U., Brueggemann, N., Zechmeister-Boltenstern, S., Williams, J., O'Dowd, C., Facchini, M. C., de Leeuw, G., Flossman, A., Chaumerliac, N., and Erisman, J. W.: Atmospheric

ACPD
14, 22793–22836, 2014

composition change: ecosystems-atmosphere interactions, Atmos. Environ., 43, 5193–5267, doi:10.1016/j.atmosenv.2009.07.068, 2009. 22796
Fuhrer, J.: Ozone risk for crops and pastures in present and future climates, Naturwissenschaften, 96, 173–194, doi:10.1007/s00114-008-0468-7, 2009. 22795
Ganzeveld, L., Helmig, D., Fairall, C. W., Hare, J., and Pozzer, A.: Atmosphere-ocean ozone exchange: a global modeling study of biogeochemical, atmospheric, and waterside turbulence dependencies, Global Biogeochem. Cy., 23, GB4021, doi:10.1029/2008GB003301, 2009. 22796, 22805, 22813
Gerosa, G., Derghi, F., and Cieslik, S.: Comparison of different algorithms for stomatal ozone flux determination from micrometeorological measurements, Water Air Soil Pollut., 179, 309–321, doi:10.1007/s11270-006-9234-7, 2007. 22825
Giannakopoulos, C., Chipperfield, T. P., Law, K. S., and Pyle, J. A.: Validation and intercomparison of wet and dry deposition schemes using Pb-210 in a global three-dimensional off-line chemical transport model, J. Geophys. Res.-Atmos., 104, 23761–23784, doi:10.1029/1999JD900392, 1999. 22796
Hauglustaine, D. A., Hourdin, F., Jourdain, L., Filiberti, M. A., Walters, S., Lamarque, J. F., and Holland, E. A.: Interactive chemistry in the Laboratoire de Meteorologie Dynamique general circulation model: description and background tropospheric chemistry evaluation, J. Geophys. Res.-Atmos., 109, D04314, doi:10.1029/2003JD003957, 2004. 22823
Horowitz, L. W., Walters, S., Mauzerall, D. L., Emmons, L. K., Rasch, P. J., Granier, C., Tie, X., Lamarque, J.-F., Schultz, M. G., Tyndall, G. S., Orlando, J. J., and Brasseur, G. P.: A global simulation of tropospheric ozone and related tracers: description and evaluation of MOZART, version 2, J. Geophys. Res., 108, 4784–4813, doi:10.1029/2002JD002853, 2003. 22823
Huijnen, V., Williams, J., van Weele, M., van Noije, T., Krol, M., Dentener, F., Segers, A., Houweling, S., Peters, W., de Laat, J., Boersma, F., Bergamaschi, P., van Velthoven, P., Le Sager, P., Eskes, H., Alkemade, F., Scheele, R., Nédélec, P., and Pätz, H.-W.: The global chemistry transport model TM5: description and evaluation of the tropospheric chemistry version 3.0, Geosci. Model Dev., 3, 445–473, doi:10.5194/gmd-3-445-2010, 2010. 22823
Kaminski, J. W., Neary, L., Struzewska, J., McConnell, J. C., Lupu, A., Jarosz, J., Toyota, K., Gong, S. L., Côté, J., Liu, X., Chance, K., and Richter, A.: GEM-AQ, an on-line global multiscale chemical weather modelling system: model description and evaluation of gas phase chemistry processes, Atmos. Chem. Phys., 8, 3255–3281, doi:10.5194/acp-8-3255-2008, 2008. 22823

ACPD
14, 22793–22836, 2014

Lamarque, J.-F., Emmons, L. K., Hess, P. G., Kinnison, D. E., Tilmes, S., Vitt, F., Heald, C. L., Holland, E. A., Lauritzen, P. H., Neu, J., Orlando, J. J., Rasch, P. J., and Tyndall, G. K.: CAM-chem: description and evaluation of interactive atmospheric chemistry in the Community Earth System Model, Geosci. Model Dev., 5, 369–411, doi:10.5194/gmd-5-369-2012, 2012. 22823

Lelieveld, J. and Dentener, F. J.: What controls tropospheric ozone?, J. Geophys. Res., 105, 3531–3551, doi:10.1029/1999JD901011, 2000. 22795

Loveland, T. R., Reed, B. C., Brown, J. F., Ohlen, D. O., Zhu, Z., Yang, L., and Merchant, J. W.: Development of a global land cover characteristics database and IGBP DISCover from 1 km AVHRR data, Int. J. Remote Sens., 21, 1303–1330, doi:10.1080/014311600210191, 2000. 22802

Mikkelsen, T. N., Ro-Poulsen, H., Pilegaard, K., Hovmand, M. F., Jensen, N. O., Christensen, C. S., and Hummelshoej, P.: Ozone uptake by an evergreen forest canopy: temporal variation and possible mechanisms, Environ. Pollut., 109, 423–429, doi:10.1016/S0269-7491(00)00045-2, 2000. 22825

Mikkelsen, T. N., Ro-Poulsen, H., Hovmand, M. F., Jensen, N. O., Pilegaard, K., and Egelov, A. H.: Five-year measurements of ozone fluxes to a Danish Norway spruce canopy, Atmos. Environ., 38, 2361–2371, doi:10.1016/j.atmosenv.2003.12.036, 2004. 22825

Munger, J. W., Wofsy, S. C., Bakwin, P. S., Fan, S. M., Goulden, M. L., Daube, B. C., Goldstein, A. H., Moore, K. E., and Fitzjarrald, D. R.: Atmospheric deposition of reactive nitrogen oxides and ozone in a temperate deciduous forest and a subarctic woodland 1. Measurements and mechanisms, J. Geophys. Res.-Atmos., 101, 12639–12657, doi:10.1029/96JD00230, 1996. 22825

Pitari, G., Palermi, S., Visconti, G., and Prinn, R. G.: Ozone response to a CO_2 doubling – results from a stratospheric circulation model with heterogeneous chemistry, J. Geophys. Res.-Atmos., 97, 5953–5962, 1992. 22823

Rannik, Ü., Altimir, N., Mammarella, I., Bäck, J., Rinne, J., Ruuskanen, T. M., Hari, P., Vesala, T., and Kulmala, M.: Ozone deposition into a boreal forest over a decade of observations: evaluating deposition partitioning and driving variables, Atmos. Chem. Phys., 12, 12165–12182, doi:10.5194/acp-12-12165-2012, 2012. 22825

Reich, P. B. and Amundson, R. G.: Ambient levels of ozone reduce net photosynthesis in tree and crop species, Science, 230, 566–570, doi:10.1126/science.230.4725.566, 1985. 22796

ACPD
14, 22793–22836, 2014

Rotman, D. A., Tannahill, J. R., Kinnison, D. E., Connell, P. S., Bergmann, D., Proctor, D., Rodriguez, J. M., Lin, S. J., Rood, R. B., Prather, M. J., Rasch, P. J., Considine, D. B., Ramaroson, R., and Kawa, S. R.: Global modeling initiative assessment model: model description, integration, and testing of the transport shell, J. Geophys. Res.-Atmos., 106, 1669–1691, doi:10.1029/2000JD900463, 2001. 22823

Rotman, D. A., Atherton, C. S., Bergmann, D. J., Cameron-Smith, P. J., Chuang, C. C., Connell, P. S., Dignon, J. E., Franz, A., Grant, K. E., Kinnison, D. E., Molenkamp, C. R., Proctor, D. D., and Tannahill, J. R.: IMPACT, the LLNL 3-D global atmospheric chemical transport model for the combined troposphere and stratosphere: model description and analysis of ozone and other trace gases, J. Geophys. Res.-Atmos., 109, D04303, doi:10.1029/2002JD003155, 2004. 22823

Rummel, U., Ammann, C., Kirkman, G. A., Moura, M. A. L., Foken, T., Andreae, M. O., and Meixner, F. X.: Seasonal variation of ozone deposition to a tropical rain forest in southwest Amazonia, Atmos. Chem. Phys., 7, 5415–5435, doi:10.5194/acp-7-5415-2007, 2007. 22806

Sanderson, M. G., Collins, W. J., Hemming, D. L., and Betts, R. A.: Stomatal conductance changes due to increasing carbon dioxide levels: projected impact on surface ozone levels, Tellus B, 59, 404–411, doi:10.1111/j.1600-0889.2007.00277.x, 2007. 22795

Sanderson, M. G., Dentener, F. J., Fiore, A. M., Cuvelier, C., Keating, T. J., Zuber, A., Atherton, C. S., Bergmann, D. J., Diehl, T., Doherty, R. M., Duncan, B. N., Hess, P., Horowitz, L. W., Jacob, D. J., Jonson, J. . E., Kaminski, J. W., Lupu, A., MacKenzie, I. A., Mancini, E., Marmer, E., Park, R., Pitari, G., Prather, M. J., Pringle, K. J., Schroeder, S., Schultz, M. G., Shindell, D. T., Szopa, S., Wild, O., and Wind, P.: A multi-model study of the hemispheric transport and deposition of oxidised nitrogen, Geophys. Res. Lett., 35, L17815, doi:10.1029/2008GL035389, 2008. 22797

Shindell, D. T., Grenfell, J. L., Rind, D., Grewe, V., and Price, C.: Chemistry-climate interactions in the Goddard Institute for Space Studies general circulation model: 1. Tropospheric chemistry model description and evaluation, J. Geophys. Res., 106, 8047–8075, doi:10.1029/2000JD900704, 2001. 22823

Simpson, D.: Long-period modeling of photochemical oxidants in Europe – model-calculations for July 1985, Atmos. Environ. Part A – General Topics, 26, 1609–1634, doi:10.1016/0960-1686(92)90061-O, 1992. 22795

Stevenson, D. S., Dentener, F. J., Schultz, M. G., Ellingsen, K., van Noije, T. P. C., Wild, O., Zeng, G., Amann, M., Atherton, C. S., Bell, N., Bergmann, D. J., Bey, I., Butler, T., Co-

ACPD
14, 22793–22836, 2014

fala, J., Collins, W. J., Derwent, R. G., Doherty, R. M., Drevet, J., Eskes, H. J., Fiore, A. M., Gauss, M., Hauglustaine, D. A., Horowitz, L. W., Isaksen, I. S. A., Krol, M. C., Lamarque, J. F., Lawrence, M. G., Montanaro, V., Muller, J. F., Pitari, G., Prather, M. J., Pyle, J. A., Rast, S., Rodriguez, J. M., Sanderson, M. G., Savage, N. H., Shindell, D. T., Strahan, S. E., Sudo, K., and Szopa, S.: Multimodel ensemble simulations of present-day and near-future tropospheric ozone, J. Geophys. Res.-Atmos., 111, D08301, doi:10.1029/2005JD006338, 2006. 22796, 22797, 22800, 22802

Sudo, K., Takahashi, M., Kurokawa, J.-I., and Akimoto, H.: CHASER: a global chemical model of the troposphere 1. Model description, J. Geophys. Res., 107, 4339–4359, doi:10.1029/2001JD001113, 2002. 22823

Wesely, M. L.: Parameterization of surface resistances to gaseous dry deposition in regional-scale numerical-models, Atmos. Environ., 23, 1293–1304, doi:10.1016/0004-6981(89)90153-4, 1989. 22796, 22797, 22798, 22801

Wesely, M. L. and Hicks, B. B.: A review of the current status of knowledge on dry deposition, Atmos. Environ., 34, 2261–2282, doi:10.1016/S1352-2310(99)00467-7, 2000. 22795, 22796, 22798

WHO: WHO Air quality guidelines for particulate matter, ozone, nitrogen dioxide, and sulfur dioxde, Global update 2005, Summary of risk assessment, Tech. rep., World Health Organisation, Geneva, Switzerland, 2005. 22794

Wild, O.: Modelling the global tropospheric ozone budget: exploring the variability in current models, Atmos. Chem. Phys., 7, 2643–2660, doi:10.5194/acp-7-2643-2007, 2007. 22795, 22796, 22800

Wild, O. and Prather, M. J.: Excitation of the primary tropospheric chemical mode in a global three-dimensional model, J. Geophys. Res., 105, 24647–24660, doi:10.1029/2000JD900399, 2000. 22799, 22823

Young, P. J., Archibald, A. T., Bowman, K. W., Lamarque, J.-F., Naik, V., Stevenson, D. S., Tilmes, S., Voulgarakis, A., Wild, O., Bergmann, D., Cameron-Smith, P., Cionni, I., Collins, W. J., Dalsøren, S. B., Doherty, R. M., Eyring, V., Faluvegi, G., Horowitz, L. W., Josse, B., Lee, Y. H., MacKenzie, I. A., Nagashima, T., Plummer, D. A., Righi, M., Rumbold, S. T., Skeie, R. B., Shindell, D. T., Strode, S. A., Sudo, K., Szopa, S., and Zeng, G.: Pre-industrial to end 21st century projections of tropospheric ozone from the Atmospheric Chemistry and Climate Model Intercomparison Project (ACCMIP), Atmos. Chem. Phys., 13, 2063–2090, doi:10.5194/acp-13-2063-2013, 2013. 22798, 22800, 22802

ACPD
14, 22793–22836, 2014

Zeng, G. and Pyle, J. A.: Changes in tropospheric ozone between 2000 and 2100 modeled in a chemistry-climate model, Geophys. Res. Lett., 30, 1392, doi:10.1029/2002GL016708, 2003. 22823

ACPD
14, 22793–22836, 2014

Table 1. Summary of the deposition schemes and annual total global O_3 dry deposition fluxes for 15 TF HTAP models.

Model	Annual global O_3 deposition/Tg yr^{-1} Modelled	Normalised	Reference
CAMCHEM-3311m13	861	801	Lamarque et al. (2012)
CAMCHEM-3514	818	815	Lamarque et al. (2012)
CHASER-v03	939	999	Sudo et al. (2002)
FRSGC/UCI-v01	943	938	Wild and Prather (2000)
GEMAQ-EC	878	773	Kaminski et al. (2008)
GEOSChem-v07	913	932	Bey et al. (2001)
GISS-PUCCINI-modelA	975	1313	Shindell et al. (2001)
GISS-PUCCINI-modelEaer	1112	1314	Shindell et al. (2001)
GISS-PUCCINI-modelE	1179	1312	Shindell et al. (2001)
GMI-v02f	819	833	Rotman et al. (2001)
INCA-vSSz	1256	1271	Hauglustaine et al. (2004)
LLNL-IMPACT-T5a	1000	1088	Rotman et al. (2004)
MOZARTGFDL-v2	997	1119	Horowitz et al. (2003)
STOC-HadAM3-v01	1095	1226	Collins et al. (2011)
STOCHEM-v02	834	1006	Collins et al. (1997)
TM5-JRC-cy2-ipcc-v1	844	855	Huijnen et al. (2010)
ULAQ-v02	1116	1175	Pitari et al. (1992)
UM-CAM-v01	1023	1180	Zeng and Pyle (2003)
Average ($\pm 1\sigma$)	978 ± 127	1053 ± 187	
Average seasonal amplitude*	38 ± 8	30 ± 10	
Average monthly range	38 ± 6	46 ± 7	

* Defined here as the difference in total global O_3 dry deposition between the months with highest and lowest deposition fluxes.

ACPD
14, 22793–22836, 2014

Table 2. Land cover classification for the Olson and University of Maryland data sets.

Land cover class		Abbreviation		% Area	
Olson	GLCF	Olson	GLCF	Olson	GLCF
Snow and Ice	Snow and Ice	SI	SI	2.7	3.5
Deciduous Forest	Broadleaf Deciduous Forest	DF	BD	4.9	0.7
–	High Latitude Deciduous Forest	–	HL	–	1.2
Coniferous Forest	Coniferous Evergreen Forest	CF	CE	3.1	2.5
–	Mixed Coniferous Forest and Woodland	–	MC	–	1.4
Agricultural Land, Crops	Crops	AC	CR	2.7	3.1
Grass Land	Grass Land	GL	GL	8.2	4.3
–	Wooded Grass Land	–	WG	–	4.7
Tropical Forest	Broadleaf Evergreen Forest	TF	BE	0.8	2.9
Tundra	Tundra	TN	TN	1.7	1.5
Desert	Bare ground	DT	BG	3.8	3.4
–	Shrubs, Bare Ground	–	SB	–	2.1
Wetland	–	WL	–	0.7	–
Urban	–	UB	–	0.0	–
Water	Water	WT	WT	71.2	68.6
Total				100	100

ACPD
14, 22793–22836, 2014

Table 3. Long term O_3 dry deposition measurement sites.

Site Name	Grid Reference	Landcover	Sampling Height/m	LAI	Sampling Period	Reference
Long term sites						
Ulborg (Denmark)	56°17′ N 8°25′ E	Mixed Coniferous Forest	18, 36	8	Oct 1995–Dec 2000	Mikkelsen et al. (2004, 2000)
Castel Porziano (Italy)	41°44′ N 12°24′ E	Holm Oak Forest	35	4.76	Jan 2013–Dec 2013	Fares et al. (2014)
Auchencorth Moss (Scotland)	55°47′ N 3°14′ W	Moorland	0.3–3.0	na[a]	Jan 1995–Dec 1998	Fowler et al. (2001)
Hyytiala (Finland)	61°51′ N 24°17′ E	Scots Pine Forest	23	6–8	Jan 2002–Dec 2003	Rannik et al. (2012)
Harvard Forest (MA, USA)	42°32′ N 72°11′ W	Mixed Deciduous Forest	30	3.4	Jan 1991–Dec 2011	Munger et al. (1996)
Citrus orchard (CA, USA)	36°21′ N 119°5′ W	Citrus Orchard	1.0–9.2	3.0	Oct 2009–Nov 2010	Fares et al. (2012)
Blodgett Forest (CA, USA)	38°53′ N 120°37′ W	Pine Plantation	12.5	1.2–2.9	Jan 2001–Dec 2007	Fares et al. (2010)
Short term sites						
Castel Porziano[b] (Italy)	41°43′ N 12°23′ E	Pseudo-steppe	8, 2	na	Jun 1993, May 1994	Cieslik and Labatut (1997)
Burriana (Spain)	39°55′ N 0°03′ W	Orange grove	10	na	16–29 Jul 1995 28 Apr–3 May 1996	Cieslik (2004)
Voghera (Italy)	45°01′ N 9°00′ E	Onion field	2.5	na	May–Jul 2003	Gerosa et al. (2007)
Le Dezert (France)	44°05′ N 0°43′ E	Pine forest	37	na	16–18 Apr 1997	Cieslik (2004)
Klippeneck (Germany)	48°10′ N 8°45′ E	Grass	2, 8	na	10–22 Sep 1992	Cieslik (2004)
San Pietro Capofiume (Italy)	44°39′ N 11°37′ E	Beet field	8	na	15–22 Jun 1993	Cieslik (2004)
Viols en Levant (France)	43°41′ N 3°47′ E	Mediterranean shrub	37	na	16–24 Jul 1998	Cieslik (2004)

[a] na: data not available.
[b] The short term measurements made at Castel Porziano were part of a different campaign from the long term data set and were made at a different location.

ACPD
14, 22793–22836, 2014

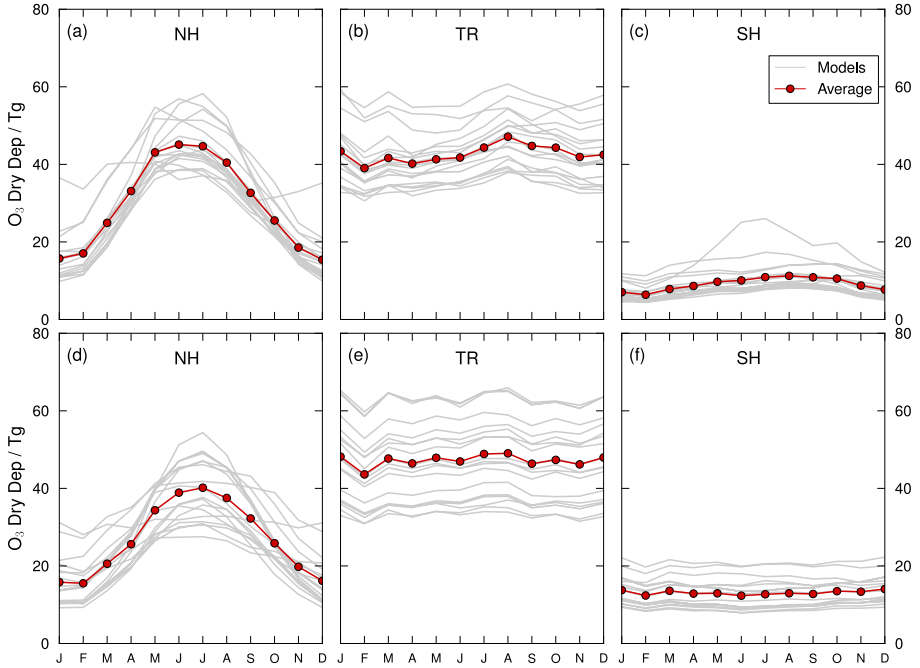

Figure 1. Modelled (top, **a**–**c**) and normalised (bottom, **d**–**f**) total monthly O_3 deposition for 15 models participating in the HTAP model intercomparison project. Modelled monthly total O_3 dry deposition is shown for the Northern Hemisphere extra-Tropics 30°–90° N **(a, d)**, Tropics 30° N–30° S **(b, e)**, and Southern Hemisphere extra-Tropics 30°–90° S **(c, f)**.

ACPD
14, 22793–22836, 2014

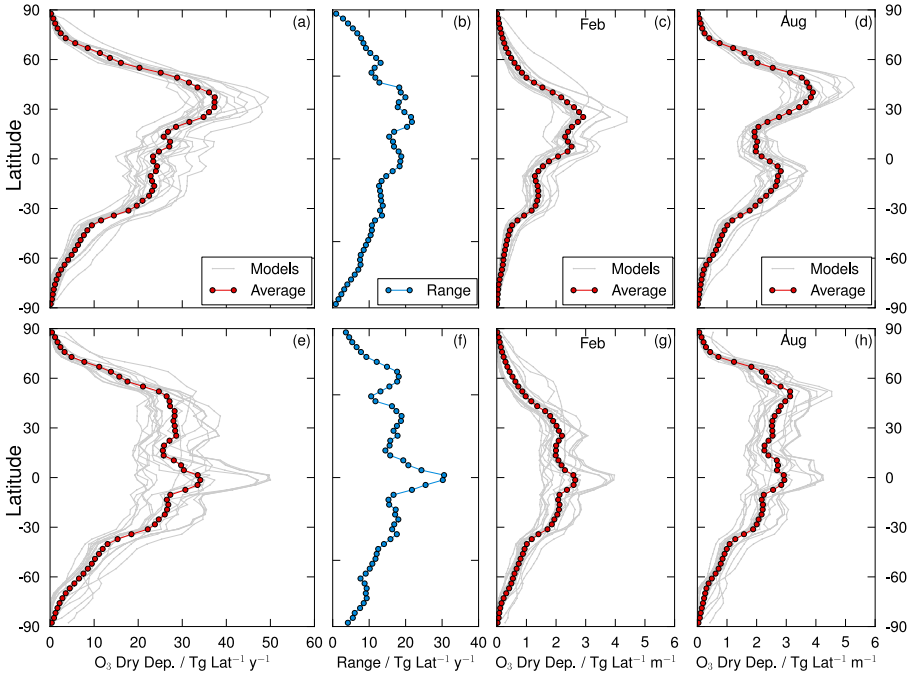

Figure 2. Latitudinal distribution of total O_3 dry deposition per 3° latitude band for the model ensemble. Modelled and normalised O_3 dry deposition fluxes are shown in the top and bottom rows respectively. Panels show the total annual O_3 dry deposition **(a, e)**, the range in annual deposition across the model ensemble **(b, f)**, and the total monthly O_3 dry deposition fluxes in February **(c, g)** and August **(d, h)**.

ACPD
14, 22793–22836, 2014

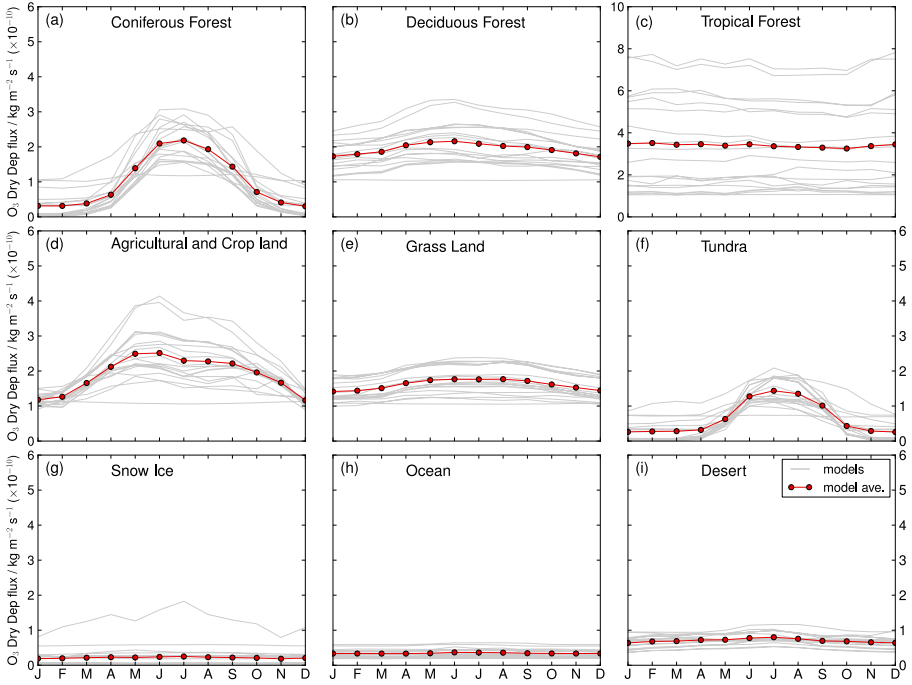

Figure 3. Normalised average monthly O_3 dry deposition at grid cells with 100 % land cover class coverage. Model fluxes are shown in grey and the ensemble average in red.

ACPD
14, 22793–22836, 2014

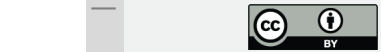

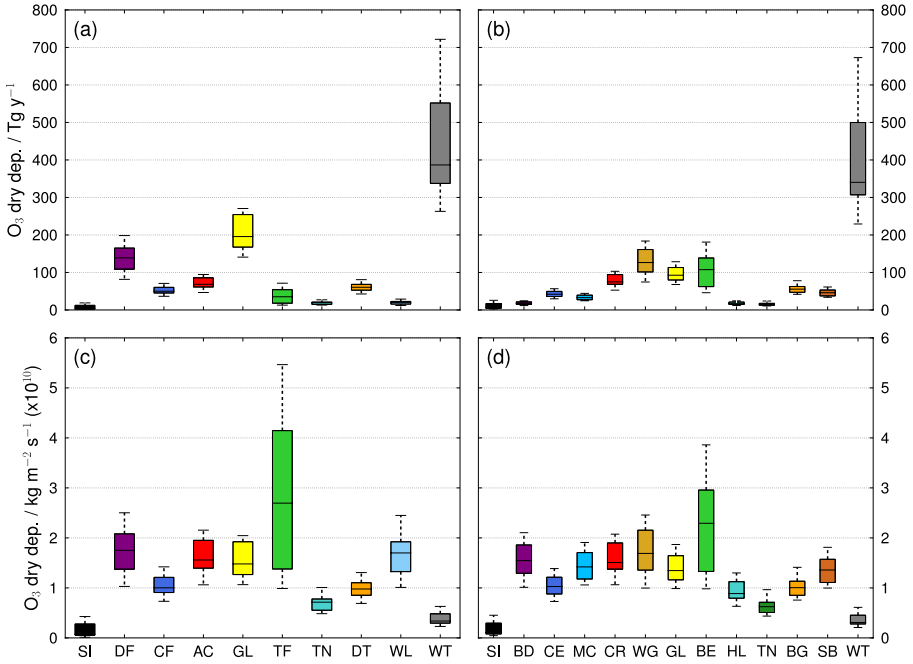

Figure 4. Normalised O_3 dry deposition partitioned to land cover classes using the OW11 **(a, c)** and GCLF **(b, d)** LCCs respectively. Upper panels show the contribution of each LCC to the annual global O_3 dry deposition flux, and lower panels show the average flux to each LCC. The box and whiskers for each land class represent the median, quartiles and 10th/90th percentiles.

ACPD
14, 22793–22836, 2014

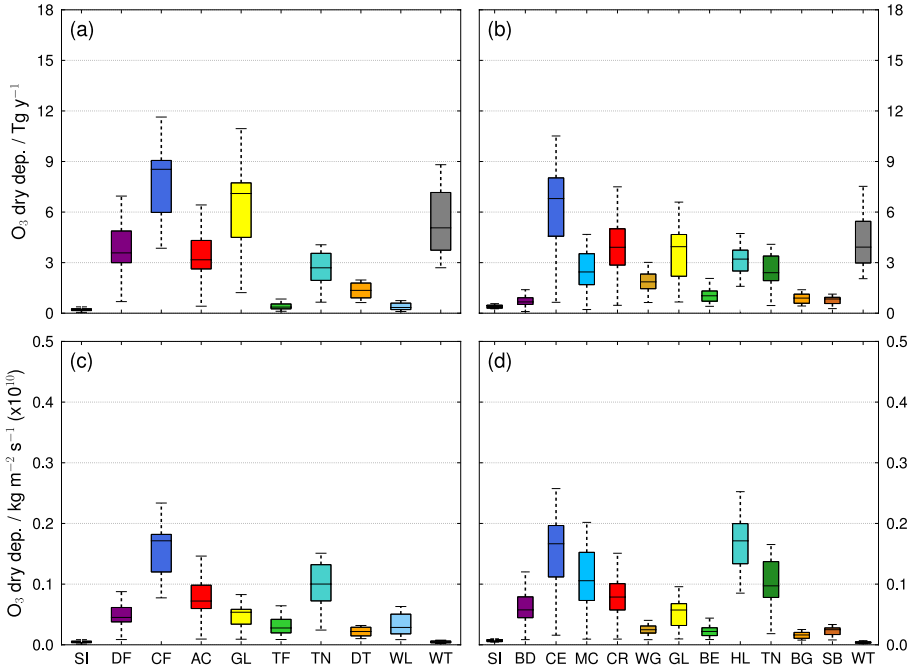

Figure 5. Seasonal amplitude in global O_3 dry deposition fluxes partitioned to the OW11 **(a)** and GCLF **(b)** land cover classes. The monthly range in average O_3 dry deposition flux is shown in the lower panels for OW11 **(c)** and GCLF **(d)** land cover classes. The box and whiskers represent the median, quartiles and 10th/90th percentiles over the model ensemble.

ACPD
14, 22793–22836, 2014

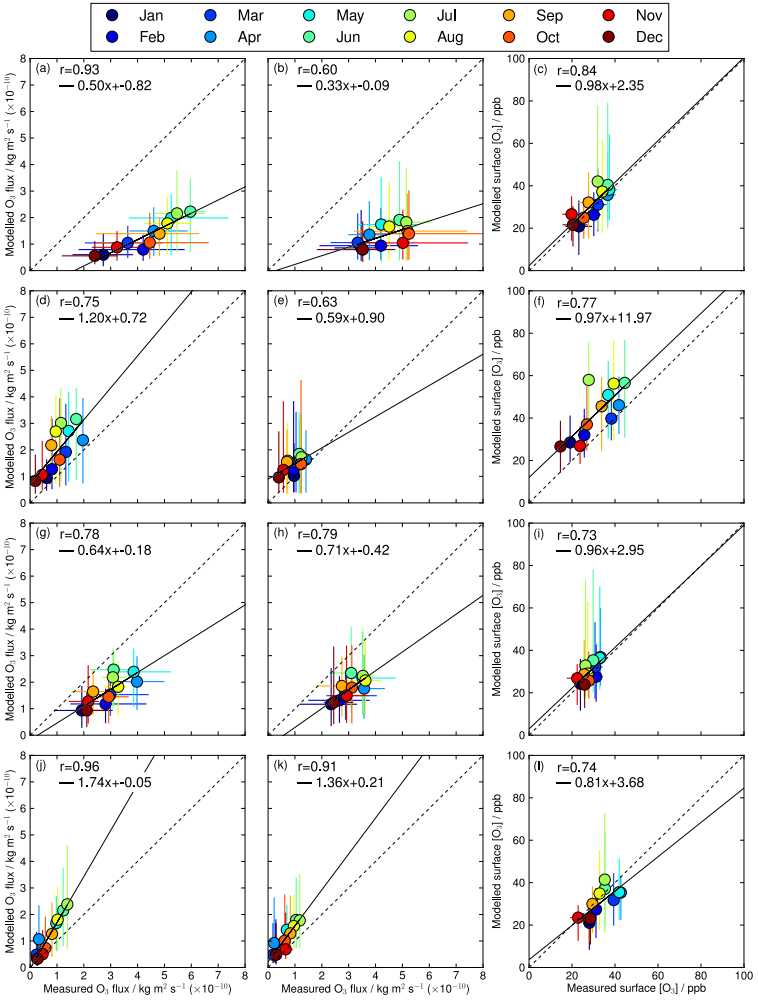

ACPD
14, 22793–22836, 2014

An evaluation of ozone dry deposition in global scale chemistry climate models

C. Hardacre et al.

Figure 6. Comparison of observed and modelled monthly average O_3 dry deposition fluxes at European sites. Individual sites are shown by row for Ulborg **(a–c)**, Castel Porziano **(d–f)**, Auchencorth Moss **(g–i)**, and Hyytiala; **(j–l)**. Observed and modelled fluxes at each site are compared directly in the left hand column, normalised fluxes are shown in the middle column, and surface O_3 is compared in the right hand column. Vertical bars represent the range in monthly flux or O_3 across the models and horizontal bars represent the interannual range in the observations, where available.

ACPD
14, 22793–22836, 2014

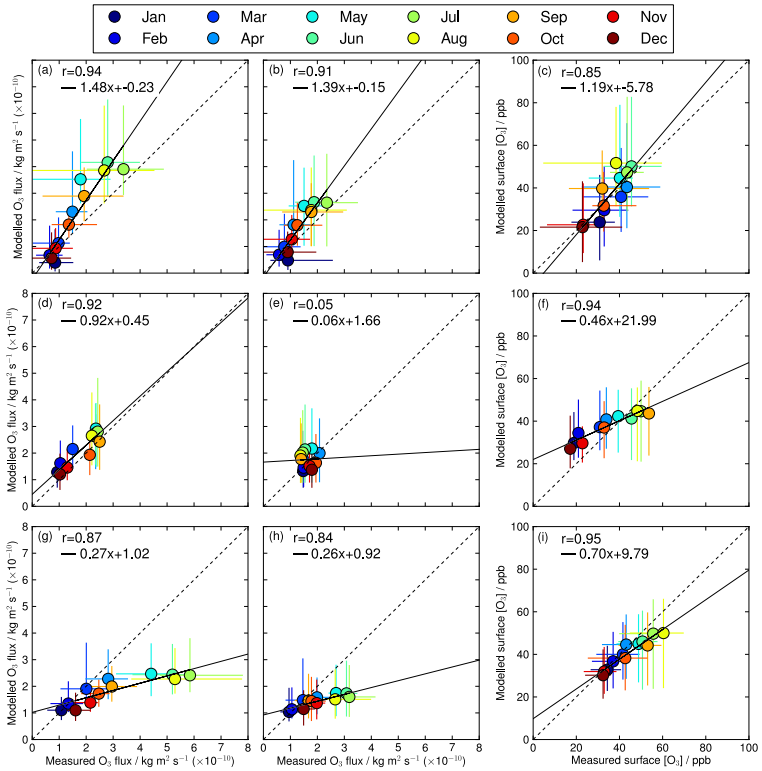

Figure 7. As Fig. 6 for North American sites. From top to bottom Harvard Forest **(a–c)**, Californian citrus orchard **(d–f)**, and Blodgett Forest **(g–i)**.

ACPD
14, 22793–22836, 2014

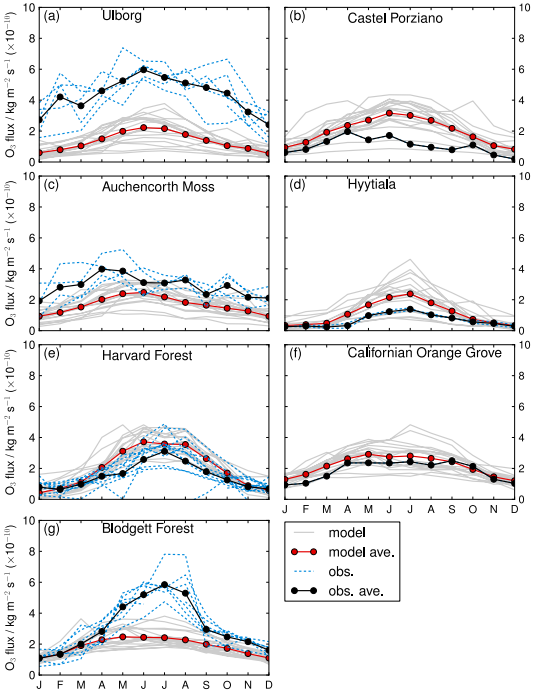

Figure 8. Measured and modelled monthly average O_3 dry deposition fluxes at Ulborg **(a)**, Castel Porziano **(b)**, Auchencorth Moss **(c)**, Hyytiala **(d)**, Harvard Forest **(e)**, Californian orange grove **(f)**, and Blodgett Forest **(g)**.

ACPD
14, 22793–22836, 2014

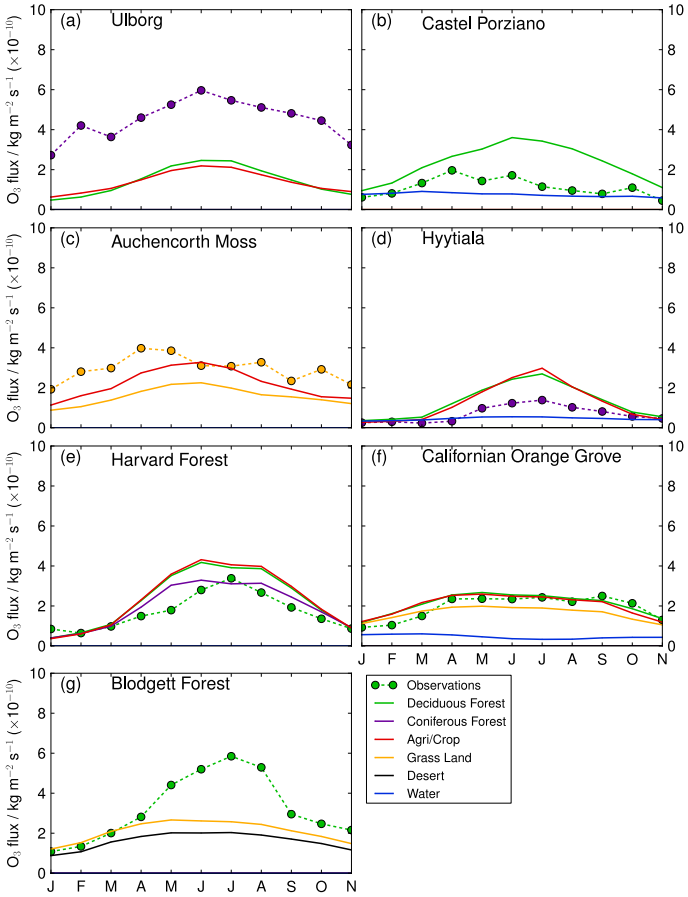

Figure 9. Observed monthly average O_3 dry deposition fluxes at measurement sites (dashed lines) and repartitioned model fluxes for each land cover class (solid lines). Colours indicate the LCC at the site and in the model grid cell containing the site.

ACPD
14, 22793–22836, 2014

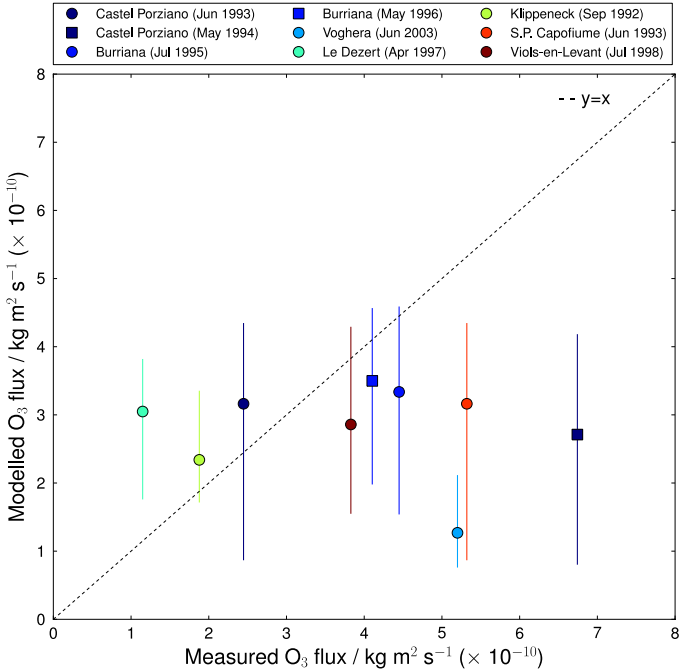

Figure 10. Measured and modelled monthly average O_3 dry deposition fluxes at short-term measurement sites in Europe.

ACPD
14, 22793–22836, 2014